Powder Technology 392 (2021) 570–586

Contents lists available at ScienceDirect

Powder Technology

journal homepage: www.elsevier.com/locate/powtec

Numerical simulation of flow and heat transfer characteristics of nanofluids in built-in porous twisted tape tube

Yuxing Wang, Cong Qi *, Zi Ding, Jianglin Tu, Rui Zhao

School of Electrical and Power Engineering, China University of Mining and Technology, Xuzhou 221116, China

ARTICLE INFO

Article history:
Received 9 June 2021
Received in revised form 18 July 2021
Accepted 21 July 2021
Available online 24 July 2021

Keywords:
Nanofluids
Forced convection
Porous twisted tape
Comprehensive evaluation index

ABSTRACT

For enhancing the heat transfer efficiency of heat exchanger, silica-water (SiO_2-H_2O) nanofluids were used as a working medium in this study. Further, the effects of tube structure, twisted tape hole spacing, and hole shape on the flow and heat exchange characteristics of nanofluids in the tube were systematically researched by numerical simulation. The results displayed that a triangular tube exhibited larger flow resistance, better heat transfer effect and more comprehensive performance compared to the round tube. The conclusion also showed that the highest comprehensive evaluation index (PEC) was obtained by producing open circular holes on the twisted tape. The usage of porous twisted tape, nanofluids, and triangular tube could significantly improve the system economy and enhance the heat exchange ability. At the same time, the flow in the tube was disordered and accompanied with the increase in entropy. The maximum improvement of heat exchange efficiency of nanofluids in round tube and triangular tube with porous twisted tape was 74.80 and 55.97%, respectively.

1. Introduction

With the development of heat transfer equipment technology and simultaneous increase in prominent energy problem, conventional heat transfer media and equipment no longer meet the requirement of high-efficiency heat exchange, thus the scientists devote extensive research efforts to actively seek new heat transfer media and equipment. As a new working medium, nanofluids have been extensively and comprehensively studied and applied in numerous fields [1], such as solar photothermal conversion [2–4], phase change heat transfer [5–9], forced heat transfer [10–15], water preparation [16,17], natural convection heat exchange [18–21], electronic component heat transfer [22–25], and magnetic nanofluids [26–28].

Till date, extensive research efforts have been devoted to the study on flow and heat exchange of nanofluids. For instance, Kristiawan et al. [29,30] put forward the investigation on influence of different concentrations of TiO2/water nanofluids on the heat transfer mechanism by studying the forced convection heat transfer and hydraulic performance of nanofluids. Afrand et al. [31,32] predicted the viscosity of nanofluids by curve fitting, and put forward a new experimental variable correlation. Harandi et al. [33–35] studied the correlation between the volume fraction of nanofluids and thermal conductivity, and put forward an accurate formula to predict the relationship between them through experimental measurement. Li et al. [36,37] studied the change in flow and heat transfer characteristics of nanofluids by adjusting the wall shape and adding helical turbulator in the flow channel, and further obtained the system feedback under different working conditions. Izadi et al. [38–40] studied the natural convection of nanofluids, analyzed the heat exchange characteristics in the cavity by changing the magnetic field, porous medium, built-in cylinder, and other conditions, and finally established a related model via numerical simulation to obtain the change rule of the average Nusselt number.

Nanofluids, as a new working medium, are also used widely in composite heat transfer enhancement technology. For example, Wijayanta et al. [41–43] studied the enhancement of heat transfer by installing porous tapes with different lengths and shapes in tubes through experiments and numerical simulation, analyzed the Nusselt number and resistance coefficient, and finally obtained the accurate conclusion related to heat transfer. Qi et al. [44,45] studied the thermal–hydraulic performance of related heat pipes using nanofluids as a working medium under the conditions of pipe structure and external magnetic field. Wang et al. [46–48] combined bionic channel structure with nanofluids, coupled artificial neural network with heat exchange design in different heat transfer systems, and found that the predicted values coincided well with the experimental results. Bahiraei et al. [49,50] analyzed the characteristics of nanofluids with different particle shapes in pin-fin and shell-and-tube heat exchangers, and further studied the heat transfer coefficient, temperature, surface thermal resistance, and other parameters by numerical simulation, and thus obtained the corresponding laws.

* Corresponding author.
E-mail address: qicong@cumt.edu.cn (C. Qi).

https://doi.org/10.1016/j.powtec.2021.07.066
0032-5910/

Nomenclature

A	effective area of tube, m^2
a	side length of triangle, mm
Be	dimensionless pressure drop along a channel
b	width of steel belts, mm
c_p	specific heat of nanofluids, J kg^{-1} K^{-1}
c_{pb}	specific heat of base fluid, J kg^{-1} K^{-1}
c_{pp}	specific heat of nanoparticle, J kg^{-1} K^{-1}
D	inner diameter of holes, mm
d_c	hydraulic diameter, m
F_i	External force per unit volume, N
f	frictional resistance coefficient
f_{bf}	frictional resistance coefficient of base fluid
f_{nf}	frictional resistance coefficient of nanofluids
g_i	gravity with vector direction, m s^{-2}
h	convective heat transfer $\rho u_i \rho u_i$coefficient, W m^{-2} K^{-1}
k	thermal conductivity, W m^{-1} K^{-1}
k_f	thermal conductivity of base fluid, W m^{-1} K^{-1}
k_{nf}	thermal conductivity of nanofluids, W m^{-1} K^{-1}
k_p	thermal conductivity of nanoparticle, W m^{-1} K^{-1}
L	length of steel belts, mm
l	hole spacing, mm
Nu	Nusselt number
Nu_{bf}	Nusselt number of base fluid
Nu_{nf}	Nusselt number of nanofluids
P	wetted perimeter, m
Pr	Prandtl Number
p	pressure, Pa
Δp	pressure drop, Pa
q	energy flux vector
Q_f	effective heating power, W
Re	Reynolds number
S_m	source point
T_{wi}	temperature of inner wall, K
T_f	average temperature of nanofluids in tube, K
t	duration, s
U	energy density
u	velocity of nanofluids, m s^{-1}
u_i	velocity vector
u_j	velocity vector
x	point coordinates
Greek symbols	
ρ	density of nanofluids, kg m^{-3}
ρu_i	density of the velocity direction i, kg m^{-3}
ρu_i	density of the velocity direction j, kg m^{-3}
ρ_{bf}	density of base fluid, kg m^{-3}
ρ_p	density of nanoparticle, kg m^{-3}
ω	nanoparticle mass fraction, %
λ_f	thermal conductivity of nanofluids, W m^{-1} K^{-1}
μ_{nf}	dynamic viscosity of nanofluids, kg m^{-1} s^{-1}
μ_f	dynamic viscosity of nanofluids, kg m^{-1} s^{-1}
η	comprehensive performance index
∂	thickness of steel belts, mm
τ_{ij}	tangential stress, N
Subscripts	
bf	base fluid
nf	nanofluids
p	nanoparticle
i	vector direction
j	vector direction

As mentioned above, significant research efforts have been devoted to the research on heat exchange in smooth tubes and heat exchangers with different shapes; nonetheless, the research on flow resistance and heat transfer characteristics of triangular tubes with twisted tapes and holes has rarely been investigated. The main objective of this study was to build the flow heat transfer model of porous twisted tape in round and triangular tube by numerical simulation, and analyze the flow resistance coefficient, Nusselt number, and PEC comprehensive evaluation index. The innovation of this study is that the flow and heat transfer in tubes with different hole shapes were studied, the mechanism of twisted tapes with different hole spacing and hole shapes was revealed through numerical analysis, and the optimal solution of heat transfer enhancement structure in the tube was obtained, which is of potential guiding significance to the field of industrial heat exchangers. As one of the innovations, in this study, the entropy enhancement in the tube with the built-in porous tapes was investigated, and Bejan number (Be) was used to analyze it. It was found that triangular tubes and smaller hole spacing could obviously enhance the heat exchange characteristic, simultaneously leading to an increase in entropy. The best configuration scheme for enhancing the heat transfer of the system was obtained based on the comprehensive comparison of PEC index.

2. Physical model and numerical method

2.1. Physical model

In the field of industrial engineering, convective heat transfer of fluid in tubes is often used in heat exchangers and numerous other thermal equipment sets. Improvement in heat transfer efficiency, increase in compactness, and saving resources have become the daunting problems to be solved urgently. Compared to the original heat-exchange pipe, the heat-exchange pipe with built-in porous tapes not only improves the heat exchange efficiency, but also can be easily constructed with high application value. In this study, mainly different hole spacing and hole shapes on the twisted belts were systematically explored. The structural diagrams of different twisted belts are shown in Fig. 1. All the twisted tape models were formed using twisted steel tapes with width b = 20 mm, thickness δ = 1 mm, and length L1 = 1200 mm. There were round holes with hole spacing l = 50, 100, and 150 mm, and triangular holes and square holes with hole spacing l = 100 mm. Twisted tapes with different shapes were inserted into a round tube with length L2 = 1200 mm and inner diameter D = 24 mm and a triangular tube with the same cross-sectional area, and twisted tapes with equal proportions were inserted into the triangular tube. The same cross-sectional area instead of the perimeter was selected in this study because under the condition of constant controlled flow rate, adjusting the cross-sectional area can ensure the same inlet velocity of tubes with different shapes.

2.2. Numerical simulation method

2.2.1. Simplification and hypothesis of the model

The flow form of the fluid after the insertion of the twisted tape into the pipeline is complicated, which belongs to three-dimensional (3D) rotating flow; therefore, in order to make the model more consistent with the real flow situation and make the research problem relatively simple, the following assumptions for the model of fluid flow in the pipe are defined: (1) external factors do not influence the parameters of the working medium in the process of numerical simulation, and the fluid is incompressible Newtonian fluid with steady flow; (2) the flow and heat transfer process of working medium in the tube are steady; (3) the boundary condition of the wall is no slip; (4) the temperature of the pipe wall is constant, the twisted tape surface is insulated; (5) with reference to the flow velocity of the fluid rotating in the tube with inserted twisted tape during the industrial experiment, the flow velocity in the channel is set to be not less than 0.25 m s-1; and (6) the fluid in the pipeline completely develops turbulent flow everywhere. The numerical simulation model proposed in this study was 3D, turbulent and steady-state model, based on the finite volume

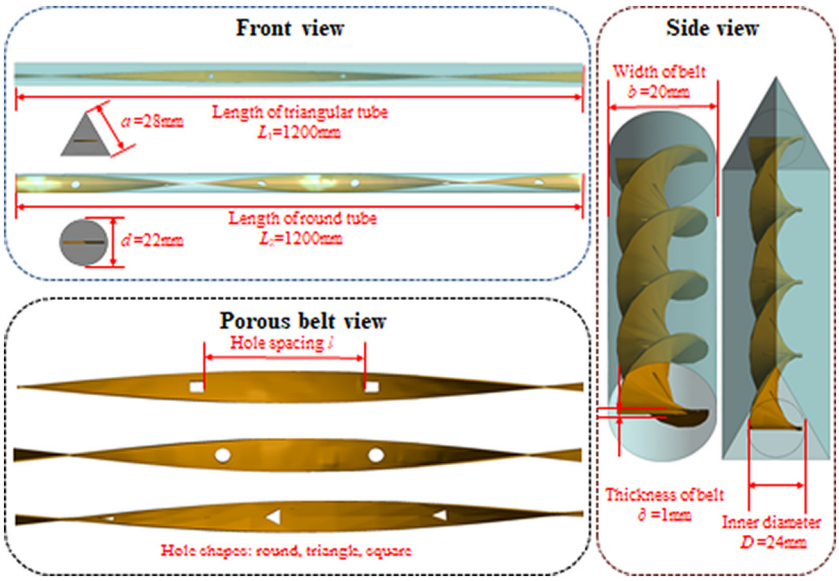

Fig. 1. Structural drawing of tubes.

method; therefore, the discrete control equation was realized by solving the pressure coupling equation semi-implicitly, and the SIMPLE algorithm was adopted. Moreover, the core of the research involves the process of guessing and correcting. This calculation method is suitable for the turbulent tube model used in this study. At the same time, the second-order upwind scheme was used to discretize the numerical values before and after the grid nodes, which were then transferred to the next node for solution.

At the same time, the specific boundary conditions are as follows: the fluid inlet adopts the velocity boundary condition, and the inlet temperature is 273 K. The boundary condition of the pipe wall is set as constant temperature, and steel is used as the pipe material, the wall temperature is constant at 303 K, being a fixed and non-slip wall condition, ignoring the thickness of the pipe wall. The surface of the porous twisted tape is set as the adiabatic wall condition in the first type of boundary condition, and the material used is also steel. At the outlet the pressure outlet boundary condition is set, the outlet pressure is set to the atmospheric pressure, and the gauge pressure is 0 Pa. This boundary condition is set for the reason that the inlet and outlet of the tube are open boundaries, and different Reynolds numbers are distinguished by controlling the inlet velocity, while the outlet is the default pressure boundary. At the same time, the wall is at a fixed temperature to heat the flow in order to obtain the change in internal temperature, and the wall surface is set as a no-slip interface to obtain the flow resistance coefficient. Noteworthy, the FLUENT simulation software cannot deal with multiphase flow at nanometer scale, and the particle size of DPM module cannot meet the requirements of nanoparticles; therefore, the relevant physical parameters of SiO2-H2O nanofluids were set in this simulation experimental measurement, and the measurement results of related parameters were introduced later. At the same time, owing to the relatively stable characteristics and superior stability of the SiO2-H2O nanofluids, the fluid in the numerical simulation could be regarded as a single-phase flow. The concentration of SiO2-H2O nanofluids used herein was differentiated by mass fraction. The density, thermal conductivity, and specific heat of the nanofluids with 1, 3, and 5% mass fractions were different, thus the concentrations of nanofluids were differentiated by modifying physical parameters when setting simulation conditions.

2.2.2. Governing equation and parameter calculation

Based on the relevant fluid mechanics theories, the flow process of fluid should follow various physical laws, while the working medium needs to meet the three governing equations including continuity equation, momentum conservation equation, and energy conservation equation when flowing in the pipeline. The basic three governing equations are described as follows:

As an expression of N-S equation in fluid mechanics, the mass difference between the flow rate of a single control body flowing into and out in unit time is equal to the mass increment of the fluid in the control body caused by density change, thus it can be considered that the condition of mass conservation is satisfied. The continuity equation is represented as Eq. (1):

$$\frac{\partial}{\partial t}(\rho_m) + \nabla\cdot\left(\rho_m \vec{v}_m\right) = \dot{m} \tag{1}$$

The momentum conservation equation is based on Eq. (2) as follows:

$$\frac{\partial}{\partial t}(\rho u_i) + \frac{\partial}{\partial x_i}\left(\rho_{u_i}\rho_{u_j}\right) = -\frac{\partial p}{\partial x_i} + \frac{\partial \tau_{ij}}{\partial x_j} + \rho g_i + F_i \tag{2}$$

The energy conservation equation is described in terms of Eq. (3):

$$\frac{\partial U}{\partial t} + \nabla\cdot q = 0 \tag{3}$$

The fluid used in this numerical simulation is SiO2-H2O nanofluids, with diameter of SiO2 nanoparticles as 30 nm, and the mass fraction of nanofluids is $\omega = 1\%$, $\omega = 3\%$, and $\omega = 5\%$, respectively. In order to accurately simulate the flow of nanofluids in the pipeline, it is necessary to calculate its physical parameters, in which the density of nanofluids can be given by the classical density formula based on Eq. (4) as follows:

$$\rho = (1-\omega)\rho_{bf} + \omega\rho_p \tag{4}$$

The empirical formula of specific calorific value of nanofluids is represented as Eq. (5):

$$c_p = (1-\omega)c_{pb} + \omega\rho_{pp} \tag{5}$$

The empirical formula for the thermal conductivity of nanofluids is expressed as Eq. (6):

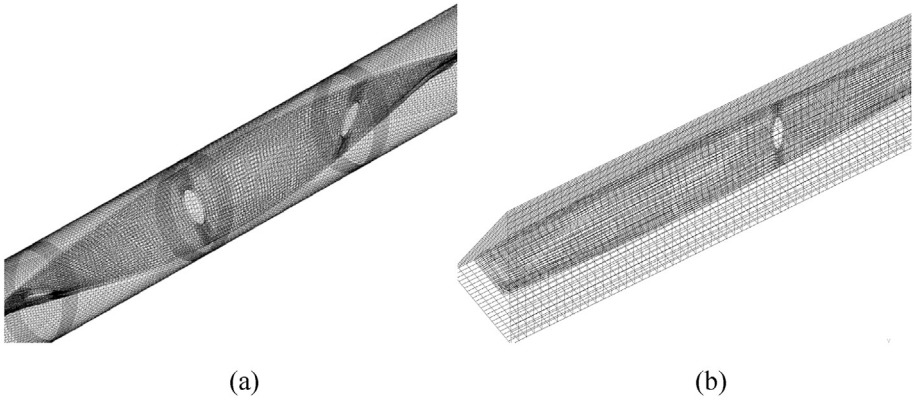

Fig. 2. Schematic illustration of grid division, (a) round tube and (b) triangular tube.

$$k_{nf} = k_f\left[\frac{(k_p + 2k_f) - 2\omega(k_f - k_p)}{(k_p + 2k_f) + \omega(k_f - k_p)}\right] \tag{6}$$

The empirical formula of hydrodynamic viscosity of nanofluids is based on Eq. (7):

$$\mu_{nf} = \frac{\mu_f}{(1-\omega)^{2.5}} \tag{7}$$

The physical values of different pipelines are given. According to the cross-sectional values, the equivalent diameter can be calculated by using the following Eq. (8):

$$d_c = \frac{4A_c}{P} \tag{8}$$

The Reynolds number *Re* is calculated as follows:

$$Re = \frac{\rho u d_c}{\mu_f} \tag{9}$$

The calculation formula of convective heat transfer coefficient is represented as follows:

$$h = \frac{Q_f}{\pi d_c l(T_{wi} - T_f)} \tag{10}$$

The formula for calculating Nusselt Number *Nu* is expressed as follows:

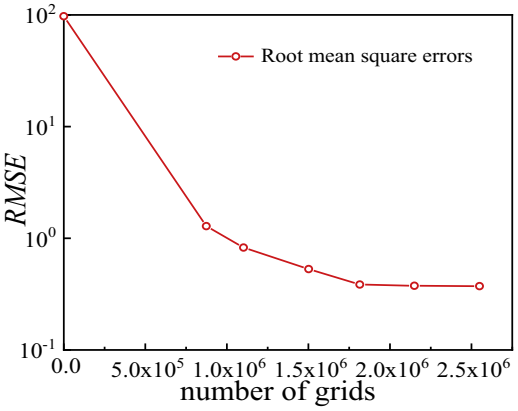

Fig. 4. Independence test chart: (a) resistance coefficient and (b) Nusselt number.

$$Nu = \frac{hd_c}{\lambda_f} \tag{11}$$

The calculation formula of resistance coefficient is represented as Eq. (12):

$$f = \frac{2d_c\Delta p}{\rho u^2 \Delta l} \tag{12}$$

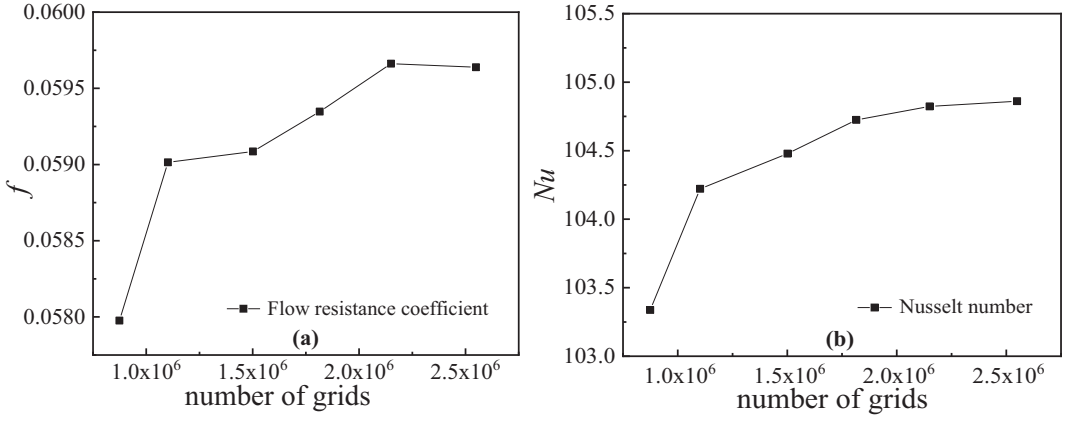

Fig. 3. Independence test chart: (a) resistance coefficient and (b) Nusselt number.

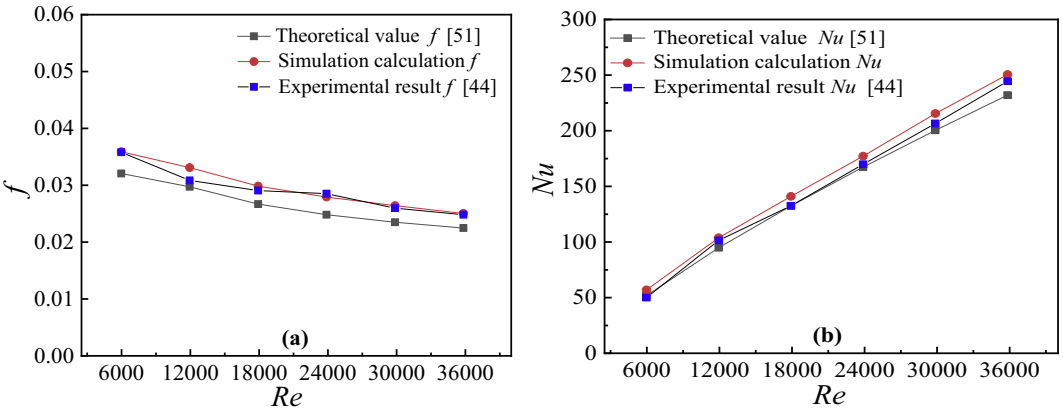

Fig. 5. Model validation: (a) resistance coefficient and (b) Nusselt number.

Table 1
Physical parameters of SiO_2-H_2O nanofluids at 300 K.

Mass fraction of SiO_2-H_2O nanofluids(%)	Density ρ (kg m^{-3})	Thermal conductivity k_{nf} (W m^{-1} K^{-1})	Specific heat c_p (kJ kg^{-1} K^{-1})	Viscosity μ_{nf} (kg m^{-1} s^{-1})
0(water)	997.1	0.613	4.179	1.37
0.1	997.73	0.629	4.176	1.37
0.3	998.25	0.635	4.172	1.37
0.5	998.72	0.640	4.170	1.38

In practical engineering, the double effects of heat exchange performance and flow resistance should be considered. In order to evaluate the comprehensive performance of heat exchange and flow resistance in more detail, PEC comprehensive performance evaluation method was introduced in this study. The calculation formula of PEC value is expressed as Eq. (13):

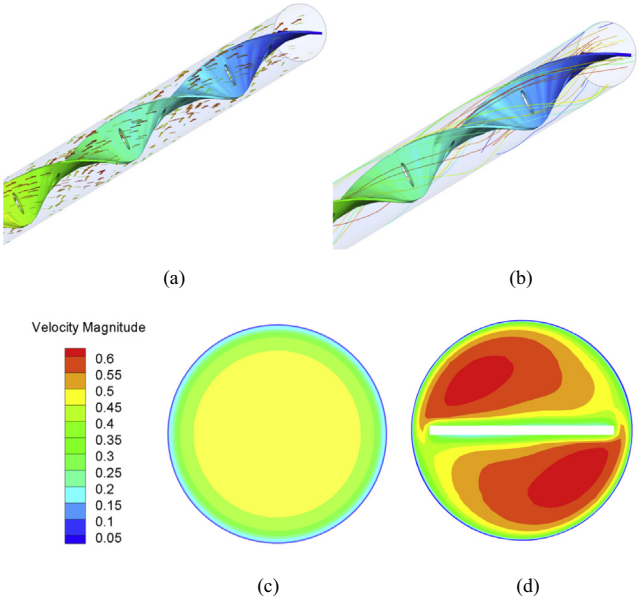

Fig. 6. Velocity-related image of round tube: (a) velocity vector, (b) velocity streamline, (c) velocity contour of round tube, and (d) velocity contour of round tube with porous twisted tape.

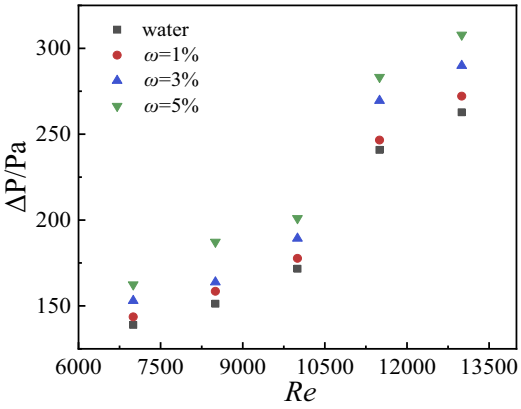

Fig. 7. Effect of mass fraction of SiO_2-H_2O nanofluids on pressure drop of round tube.

$$\eta = \left(\frac{Nu_{nf}}{Nu_{bf}}\right) / \left(\frac{f_{nf}}{f_{bf}}\right)^{\frac{1}{3}} \tag{13}$$

2.2.3. Turbulence model and near-wall area model

In the numerical simulation calculation of turbulent problems, comprehensive consideration of the suitability of different turbulence models and resources needed for calculation, and selection of the

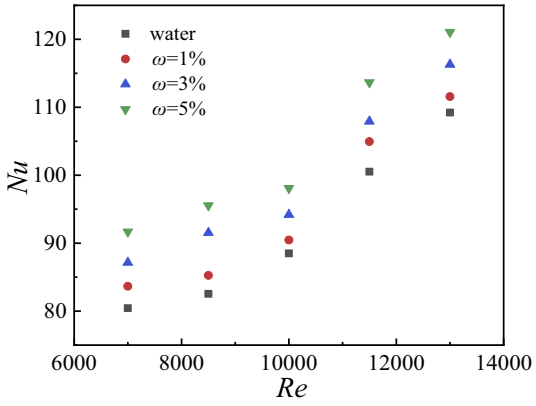

Fig. 8. Effect of mass fraction of SiO_2-H_2O nanofluids on Nusselt number of round tube.

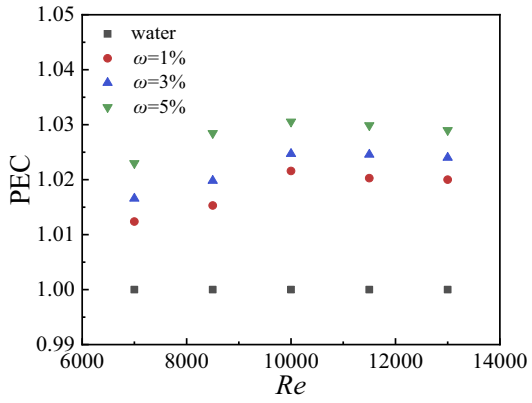

Fig. 9. Effect of mass fraction of SiO_2-H_2O nanofluids on PEC comprehensive evaluation index.

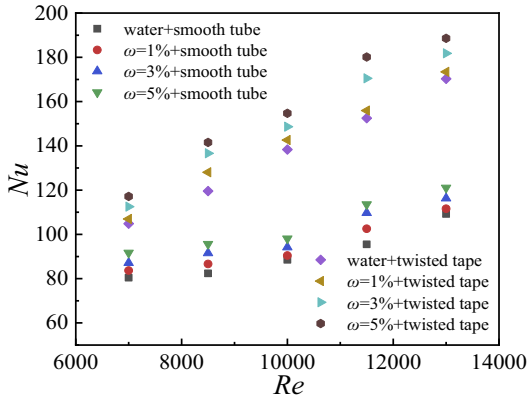

Fig. 12. Temperature contour on the axial and outlet cross-section of round tubes: (a) round tube and (b) round tube with porous twisted tape.

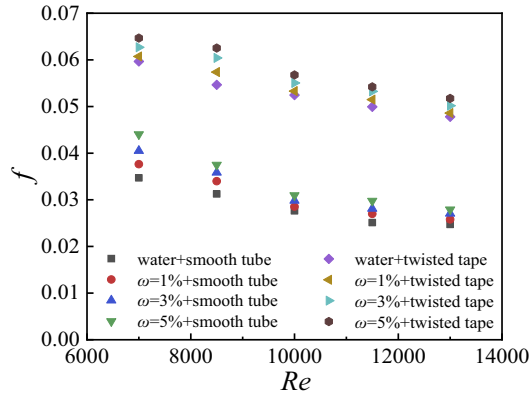

Fig. 10. Effect of volume fraction of SiO_2-H_2O nanofluids on resistance coefficient of round tube and tube with porous twisted tape.

most suitable turbulence model in numerical simulation after comprehensive evaluation are essentially required. K-ε model is a turbulence model with high stability, good economy, and accurate calculation, which is widely used. However, RNG K-ε model came into being as an improved version because of the large calculation error encountered in standard K-ε model when calculating the existing problems of vortex. Compared to the standard K-ε model, RNG K-ε model considers the rotation effect of fluid, and it has higher calculation accuracy and wider application range. Combined results of the above-mentioned analysis indicates that the fluid in the tube with the built-in porous twisted tape produces stronger rotation flow and secondary flow, and RNG K-ε model can just meet the calculation requirements. After comprehensive consideration of the factors, RNG K-ε model is selected as the turbulence model for numerical calculation of enhanced heat exchange tubes with built-in porous twisted tapes.

In general, the following two methods are available to calculate the near-wall area in fluent: wall function method and wall model method. The wall function method does not need to solve the viscous sub-layer and transition layer, and the near-wall region can be calculated and processed by using a semi-empirical formula called “wall function”, which is an approximate processing method [51]. As a semi empirical formula, it is widely used in practical industry because it can effectively calculate the shear flow problem. Its biggest advantage is that it can accurately calculate the boundary layer value without dividing very fine boundary layer mesh. This method offers broad spectrum of applications, and can deal with the numerical calculation of the flow near the wall. Considering comprehensively, this article selects the enhanced wall treatment as the treatment method of the near-wall area.

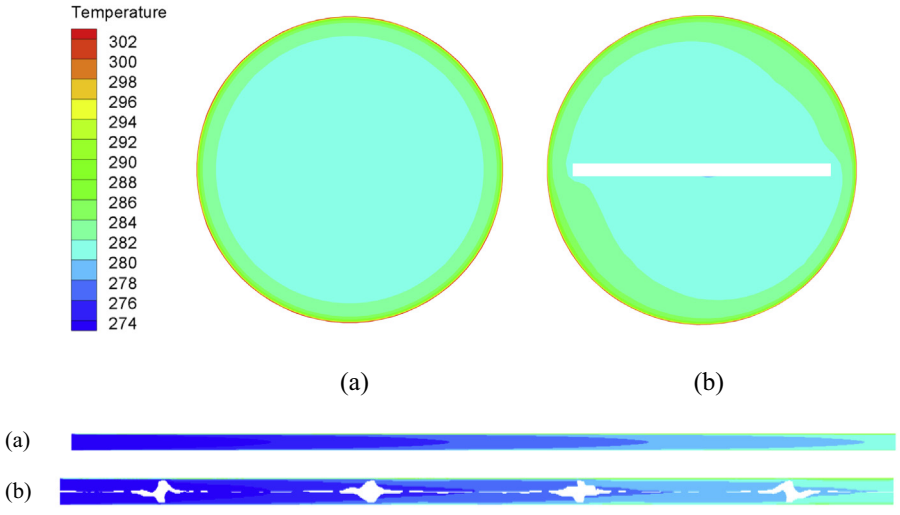

Fig. 11. Temperature contour on the axial and outlet cross-section of round tubes: (a) round tube and (b) round tube with porous twisted tape.

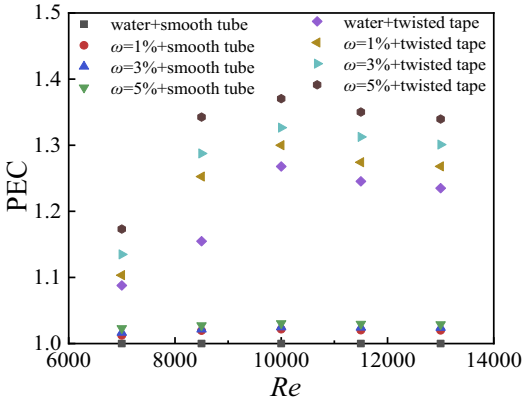

Fig. 13. Effect of volume fraction of SiO_2-H_2O nanofluids on Nusselt number of round tube and round tube with porous twisted tape.

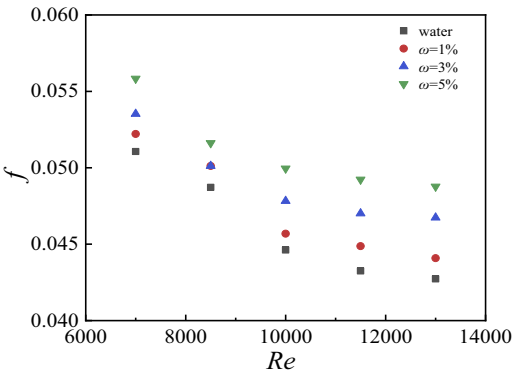

Fig. 15. Effect of volume fraction of SiO_2-H_2O nanofluids on resistance coefficient of triangular tube.

2.3. Grid division and independence verification

Considering that the flow forms involved in this study are relatively complex and have high requirements on grid quality, the grid model is obtained as shown in Fig. 2, and the grid quality of each model is kept above 0.5, which meets the calculation requirements. In the mesh drawing of this model, the total length method is adopted to encrypt the flow boundary layer of the tube, and the growth rate is set as 1.1, thus the boundary layer mesh obtained is more uniform and better in quality; moreover, the flow and heat transfer characteristics can be better analyzed during calculations.

In order to verify the independence of the grid, the six grid models with different densities are divided into 873,829, 1,101,945, 1,501,623, 1,815,225, 2,150,217, and 2,549,439 for Re = 7000. Fig. 3 presents the results of average *Nu* and f calculated by using the six calculation models with different grid numbers.

When the number of grids exceeds 2,150,217, the average deviation of *Nu* and f is not more than 0.2 and 0.1%, respectively; therefore, the calculation accuracy is sufficient at this time. Considering the calculation resources comprehensively, various models with the number of grids as 2,150,217 are employed for numerical simulation. In this study, the simulation was carried out in steady state, thus the set number of iterative steps was 3000. During calculation, it was found that the convergence position of different grid numbers was about 2100 steps, and the results of these 5 grid numbers were obtained in about 2700 steps. As a result, it was considered that the relative convergence error of different grid numbers was very small. The relative root mean square errors of convergence steps with different grid numbers were calculated quantitatively, and it was found that they were all less than 1. The corresponding results are shown in Fig. 4, which prove that the grid setting is reasonable.

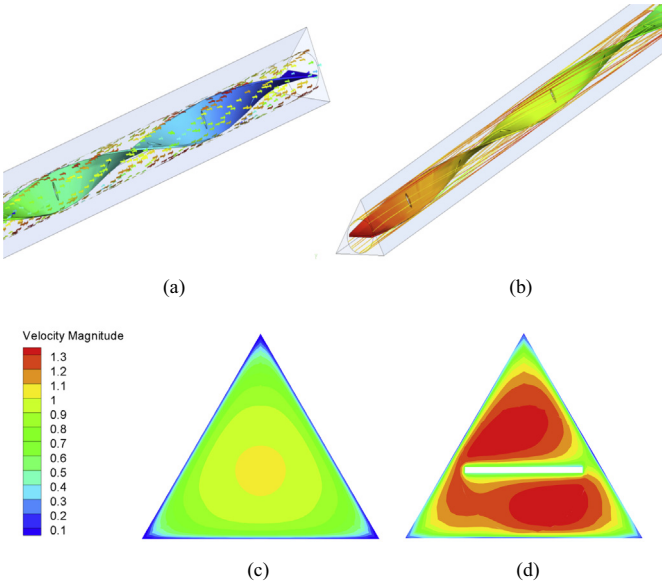

Fig. 14. Velocity-related image of triangular tube: (a) velocity vector, (b) velocity streamline, (c) velocity contour of a triangular tube, and (d) velocity contour of a triangular tube with porous twisted tape.

2.4. Reliability verification of numerical calculation

After selecting the numerical simulation method, it is also very important to verify the feasibility of the selected method. The Nusselt number and resistance coefficient used in this study were compared with those calculated by using empirical formulas. Herein, the widely accepted empirical formula was selected to calculate the theoretical Nusselt number *Nu* by using the classical Gnielinski formula [51]. Further, the Filonenko formula was used to calculate the theoretical resistance coefficient f, at the same time, the results of numerical simulation were compared with those reported by Qi et al. [44]. Fig. 5 exhibits the model validation, concluding that the curve trend is basically in accordance with the experimental results, which proves the reliability of this numerical calculation.

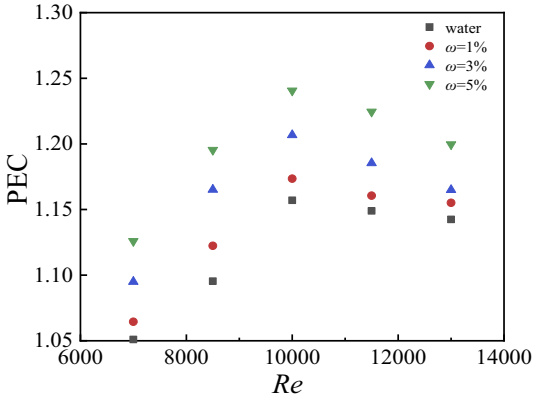

Fig. 16. Effect of volume fraction of SiO_2-H_2O nanofluids on PEC comprehensive evaluation index of triangular tube.

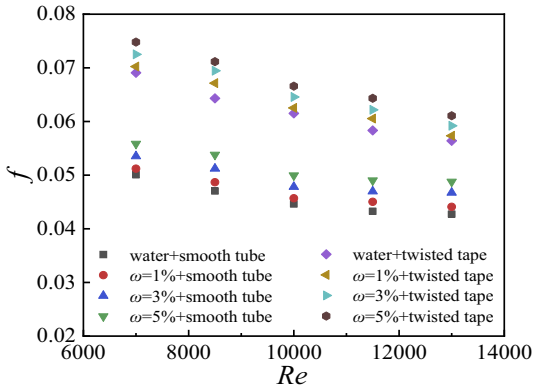

Fig. 17. Effect of volume fraction of SiO_2-H_2O nanofluids on resistance coefficient of triangular tube and triangular tube with porous twisted tape.

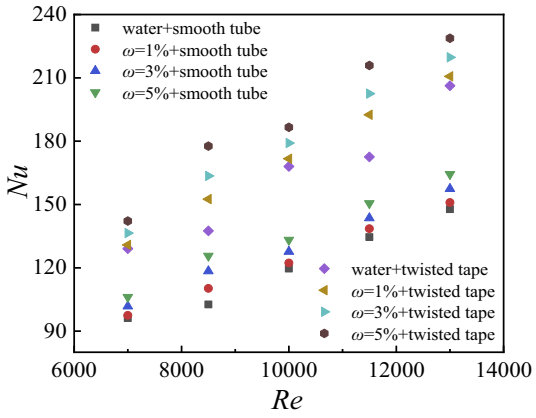

Fig. 19. Effect of volume fraction of SiO_2-H_2O nanofluids on Nusselt number of triangular tube and triangular tube with porous twisted tape.

The classical Gnielinski formula is presented as Eq. (14) [51]:

$$Nu = \frac{(f/8)(Re-1000)Pr_f}{1+12.7\sqrt{(f/8)}+\left(Pr_f^{\frac{2}{3}}-1\right)}\left[1+\left(\frac{D}{L}\right)^{\frac{2}{3}}\right]c_t \quad (14)$$

The Filonenko formula is based on Eq. (15) [51]:

$$f = (1.82 \times \lg Re - 1.62)^{-2} \quad (15)$$

3. The effects of tube structures

3.1. Heat transfer and flow characteristic of round tube

3.1.1. No built-in porous twisted tape in the tube

After the establishment of these physical models and the selection of simulation methods, the flow characteristics of SiO2-H2O nanofluids in a smooth round tube without built-in twisted tape were studied first. The physical parameters of SiO2-H2O nanofluids used in this study are listed in Table 1, and the data were obtained from previous measurements. On the premise of ensuring the lowest rotational flow rate of industrial experimental fluid and to better reflect the simulation results, numerical simulations were performed at three Reynolds numbers of 7000, 10,000, and 13,000, respectively, and the effects of different mass fractions of nanoparticles and different Reynolds numbers on the fluid flow characteristics were systematically analyzed. Figs. 6 and 7 display the velocity contour and pressure drop changes of nanofluids with different mass fractions in smooth round tubes without built-in porous twisted tape, respectively. Clearly, the figures illustrate that the velocity at the center of the tube near the twisted tape is larger, and the flow resistance increases with the increase in the mass fraction of nanoparticles. The flow resistance of nanofluids increases by 5.99, 9.44, and 12.88%, respectively, when the Reynolds number is 13000. The results indicated that the viscosity of the fluid is significantly increased after the addition of nanoparticles, and so does the resistance.

Fig. 8 demonstrates that with the increase of Reynolds number and fluid velocity, the Nusselt number also increases, and the heat exchange enhancement effect of fluid gets improved to a certain extent. The addition of SiO2 nanoparticles also leads to the increase in the Nusselt number, corresponding to the extent of heat exchange enhancement. With the increase of nanoparticle mass fraction, the heat transfer effect of fluid gradually increases, which can be increased by 10.88%, indicating that the addition of nanofluids leads to significant improvement in the heat transfer enhancement effect.

Fig. 9 shows the variation of PEC comprehensive evaluation index with Reynolds number under different mass fractions of nanofluids in smooth round tubes.

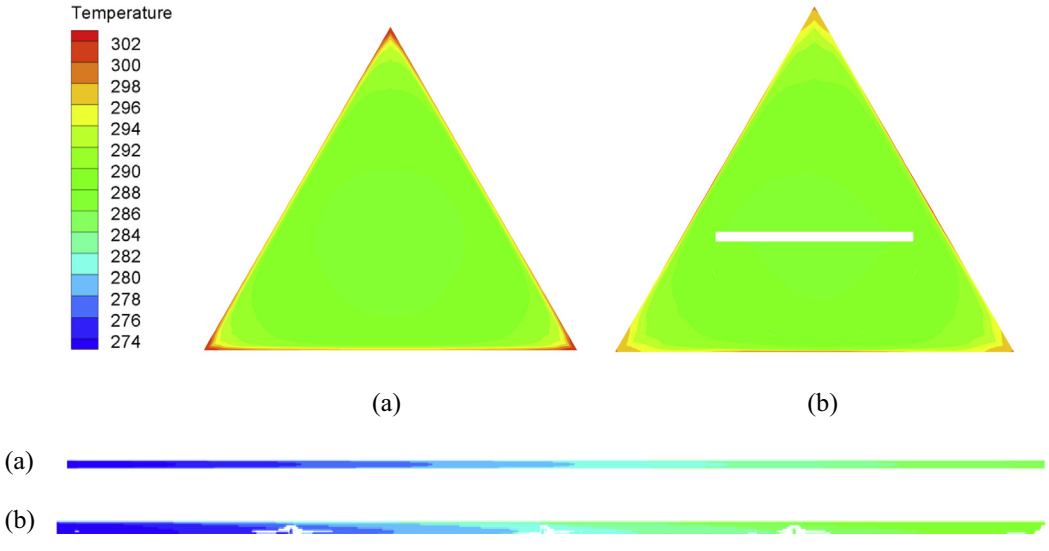

Fig. 18. Temperature contour on the axial and outlet cross-section of tubes: (a) triangular tube and (b) triangular tube with porous twisted tape.

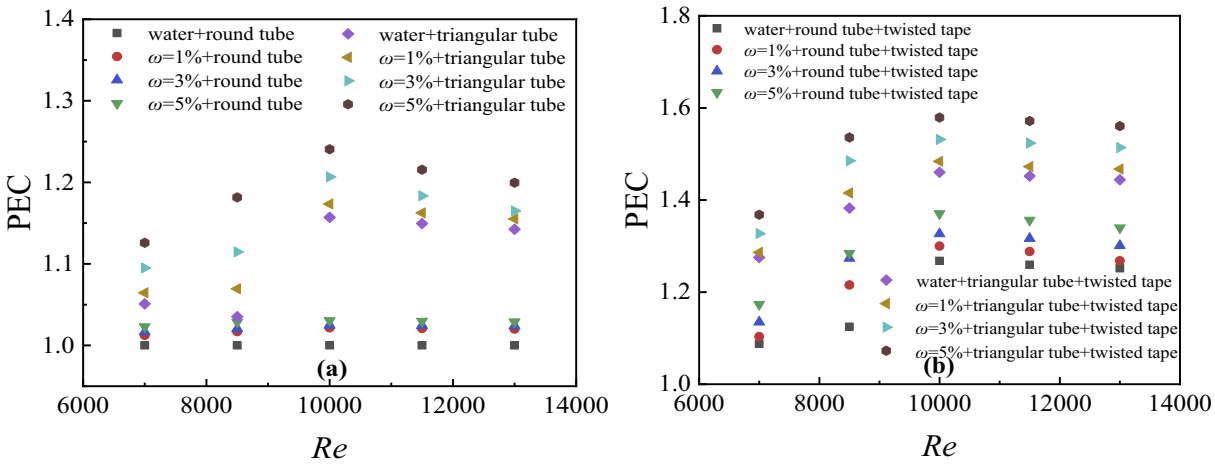

Fig. 20. Comparison of PEC comprehensive evaluation index: (a) round tube versus triangle tube and (b) round tube with porous twisted tape versus triangular tube with porous twisted tape.

On the whole, under the Reynolds number conditions simulated in this study, the PEC comprehensive evaluation index is greater than 1 after adding nanoparticles, thus indicating that the addition of nanoparticles is beneficial to improving heat exchange performance. With the increase of the mass fraction, the greater the PEC, the better the performance of the heat transfer enhancement effect. Moreover, with the increase of Reynolds number, the PEC comprehensive evaluation index shows a trend first exhibiting a rapid increase and then a decline, and the highest PEC is obtained for Reynolds number of 10,000. For Reynolds number greater than 10,000, the heat transfer enhancement effect endowed by the addition of nanoparticles is no longer obvious, and the influence of flow resistance gradually increases, which leads to the decrease of the PEC comprehensive evaluation index [52]. For the Reynolds number of around 10,000, the negative effect of flow resistance in the tube on the PEC comprehensive evaluation index of heat transfer is the least, and the heat exchange enhancement effect brought by its disturbance is the highest, thus the value of PEC peaks at this time.

3.1.2. Built-in porous twisted tape in the tube

Fig. 10 illustrates that the high-concentration nanofluids and the tube with built-in twisted tape exhibit greater resistance coefficient, because the addition of twisted tape causes friction between the fluid and the wall, which enhances the flow resistance of the fluid. At the same

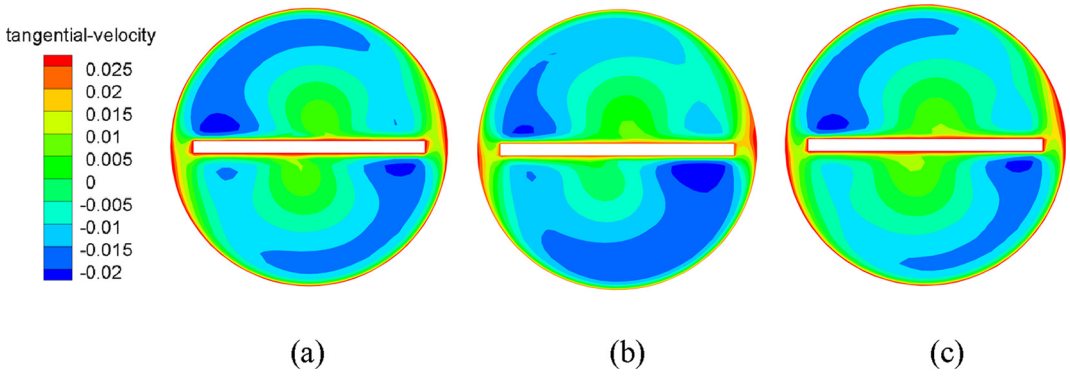

Fig. 21. The influence of different hole spacing on velocity contour of round tubes: (a) $l = 5$ cm, (b) $l = 10$ cm, and (c) $l = 15$ cm.

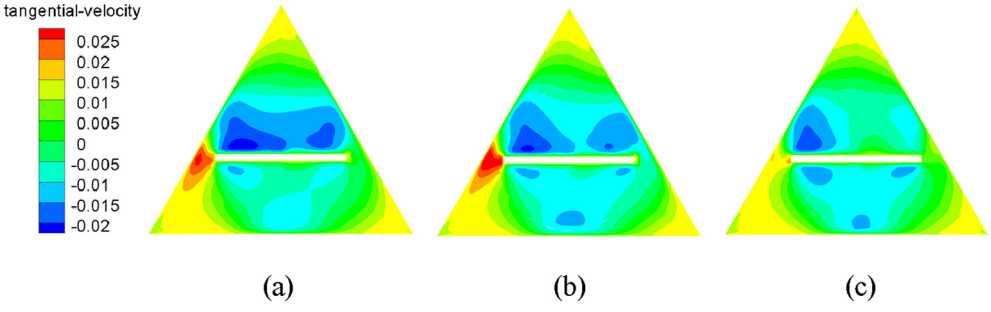

Fig. 22. The influence of different hole spacing on velocity contour of triangular tubes: (a) $l = 5$ cm, (b) $l = 10$ cm, (c) $l = 15$ cm.

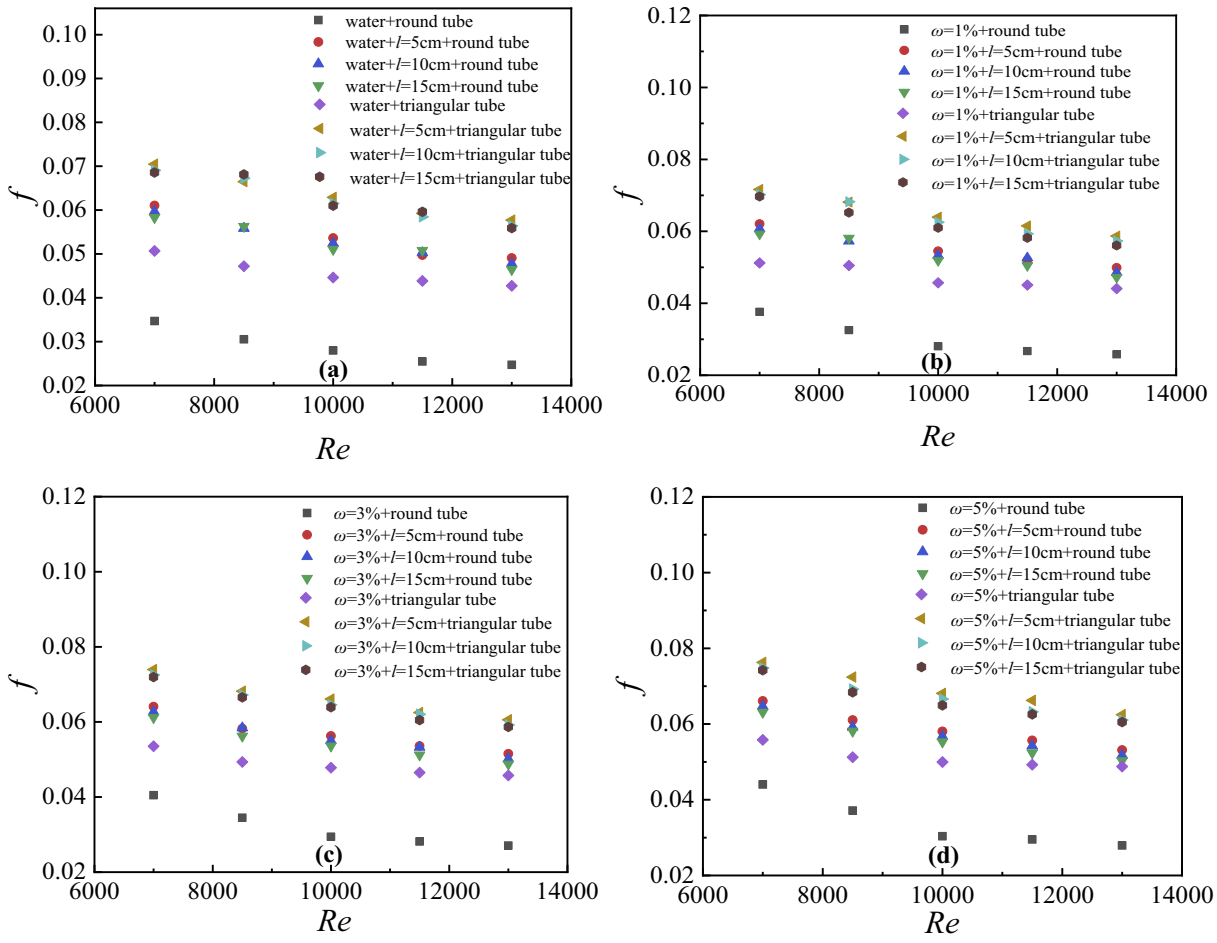

Fig. 23. The effect of hole spacing on flow resistance coefficient under different mass fraction of SiO2-H2O nanofluids: (a) φ = 0%, (b) φ = 1%, (c) φ = 3%, and (d) φ = 5%.

time, the higher viscosity of high concentration nanofluids is another important factor responsible for increasing the resistance coefficient.

Fig. 11 shows the temperature contour at the axial section and outlet of smooth round tube and tube with built-in porous twisted tape. Fig. 11 (a) exhibits that the temperature in the smooth round tube decreases gradually from the boundary area to the central area, with obvious stratification phenomenon, and the range of low temperature area is larger. However, the disturbance of the porous twisted tape disrupts the temperature stratification of fluid in the radial direction, which leads to the mixing of the fluid in the boundary area and the mainstream area, and enhances the heat exchange between the flow and the wall. After the incorporation of the porous twisted tape, the flow produces obvious radial and tangential partial velocities, which destroys the temperature stratification of the fluid in the radial direction, thus realizing heat transfer enhancement.

Fig. 12 demonstrates that with the increase of Reynolds number, the Nusselt number of each working condition also increases, and the Nusselt number of the pipe with built-in porous twisted tape is obviously larger than that of the smooth round pipe. On the one hand, the incorporation of porous twisted tape splits the flow channel, reduces the equivalent diameter of the pipe, increases the flow velocity of the fluid under the same pump power, and finally increases the disturbance of the flow. Furthermore, the porous twisted tape leads to the generation of a split flow in the radial and tangential directions, also known as the secondary flow, which is conducive to the mutual mixing of the two areas of fluid and destroys the temperature stratification, reduces the thickness of the fluid velocity boundary layer, and makes the heat exchange performance more superior. On the other hand, the enhancement of heat transfer and flow after adding twisted tape also exhibits the phenomenon of entropy increase in the flow process of the built-in pipeline. Analysis of the Bejan number [53,54] expressed in Eq. (16) represents the dimensionless pressure drop along the channel, where the L represents the flow characteristic length, μ represents the dynamic viscosity and ν represents the momentum diffusivity of flow. With the increase of pressure drop, the flow in the pipeline becomes more disordered, which disrupts the flow and enhances the heat transfer to a certain extent. Simultaneously, the corresponding diffusivity of the fluid increases due to the enhancement of heat transfer, thus the value of Be increases and the entropy increase phenomenon becomes more obvious.

$$Be = \frac{\Delta p L^2}{\mu \nu} \tag{16}$$

Fig. 13 shows the effect of volume fraction of SiO2-H2O nanofluids on PEC comprehensive coefficient of round tube and round tube with porous twisted tape. With the increase of Reynolds number, initially the PEC increases rapidly and then decreases slowly. Therefore, a critical Reynolds number exists accordingly, and the highest value of PEC can thus be obtained. When the Reynolds number is 10000 and the mass

Table 2
The change of average temperature of fluid with the hole spacing.

Hole spacing	l = 5 cm	l = 10 cm	l = 15 cm
Temperature of flow in round tube (K)	278.1387	278.1261	278.1125
Temperature of flow in triangular tube (K)	282.7678	282.7017	282.6483

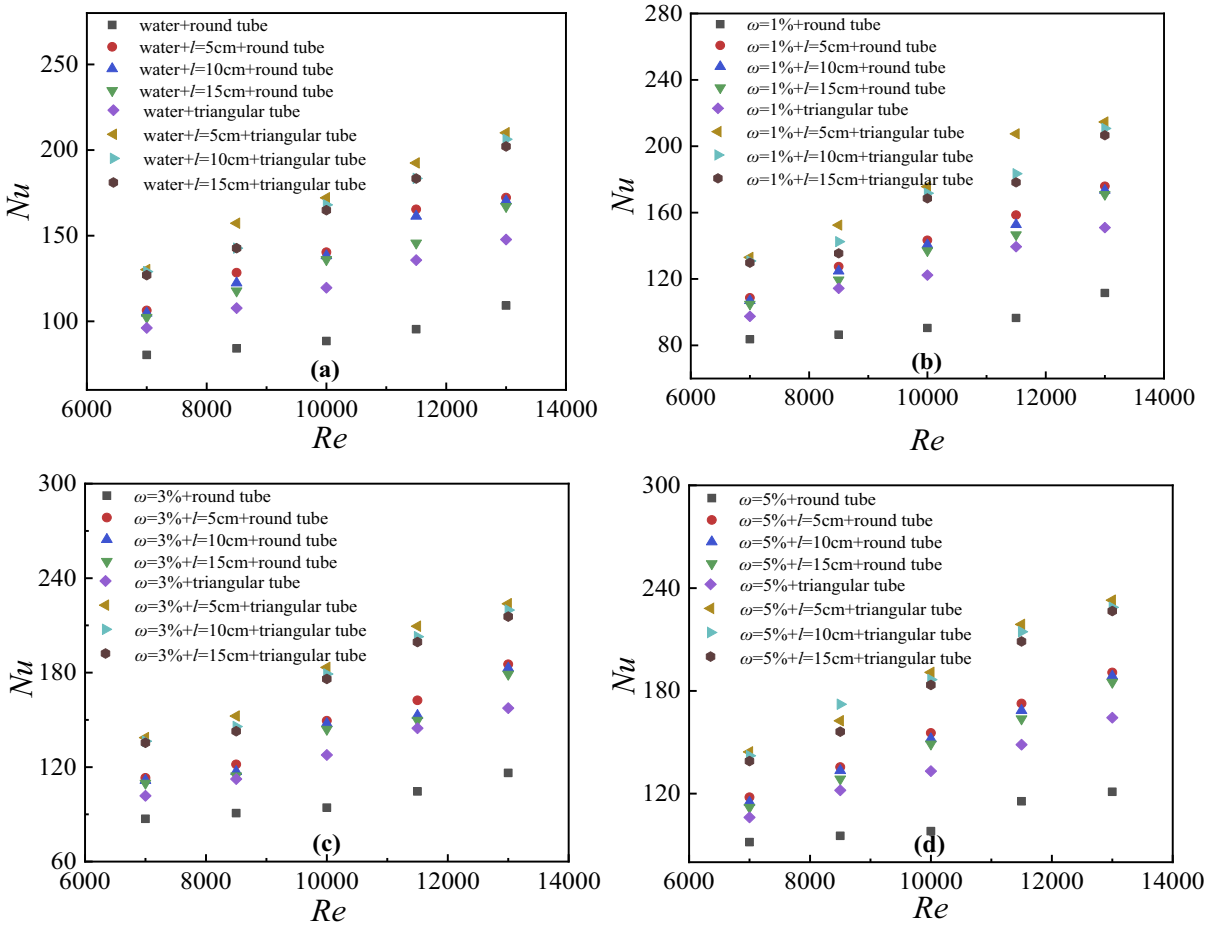

Fig. 24. The effect of hole spacing on Nusselt number under different mass fractions of SiO_2-H_2O nanofluids: (a) $\varphi = 0\%$, (b) $\varphi = 1\%$, (c) $\varphi = 3\%$, and (d) $\varphi = 5\%$.

fraction of nanoparticles is 5%, the maximum PEC composite coefficient is 1.370, which indicates that the usage of porous twisted tape and nanofluids can significantly improve the flow and heat exchange performance of the heat exchange tube.

3.2. Heat transfer and flow characteristic of triangular tube

3.2.1. No built-in porous twist tape in the tube

Based on the above-mentioned analysis and investigations carried out in round tubes, the resistance coefficient f was selected as the standard parameter to further evaluate the flow characteristics. The Reynolds numbers of nanofluids in smooth triangular tubes with the same cross-sectional area as the round tubes were numerically simulated at 7000, 8500, 10,000, 11,500, and 13,000, respectively, and the different mass fraction of nanoparticles was analyzed. Moreover, the effect of different values of Reynolds number on the flow characteristics was also systematically explored. Comparative analysis of Figs. 14 and 15 indicates that the insertion of the twisted tape leads to the significant increase in the velocity of the flow near it. Moreover, with the continuous increase of fluid velocity and Reynolds number, the resistance coefficient calculated via numerical simulation decreases continuously, and presents the same trend as the flow in the round tube, i.e., the declining rate slows down. This may be attributed to the fact that with the increase of flow velocity, the viscous boundary layer in the tube is destroyed, which causes this phenomenon to occur. When the Reynolds number is 13000, the resistance coefficient of 5% nanofluids is 15.02% higher than that of pure water.

Furthermore, the heat transfer characteristics of the triangular tube were analyzed. Fig. 16 demonstrates that with the increase of Reynolds number, the Nusselt number also increases; moreover, the Nusselt number of nanofluids with high mass fraction is greater. Analysis of the PEC comprehensive evaluation index shown in Fig. 16 indicates that the PEC increases rapidly, and then decreases slowly. The Reynolds number of 10,000 indicates the peak point of PEC comprehensive evaluation index. Compared to the PEC of round tube, the value of triangular tube is larger, which indicates that triangular tube shows a better heat exchange effect.

3.2.2. Built-in porous twist tape in the tube

Fig. 17 shows the changing trend of flow resistance, revealing that the trends of the two tubes are basically the same, i.e., the resistance coefficient decreases with the increase of Reynolds number. When Reynolds number is 13000, the flow resistance coefficient of the built-in porous twist tape tube with 5% mass fraction of nanoparticles is 42.91% higher than that of the smooth triangle tube. This may lead to the division of the cross-sectional area in the tube, thus the flow velocity increases, and the complicated pipeline structure enhances the disturbance, which leads to the increase in the flow resistance.

Fig. 18 shows the temperature contour on the axial and outlet cross-section of triangular tube and on the triangular tube with porous twisted tape. The figure illustrates that the temperature distribution in the tube is lower in the mainstream area and higher in the boundary area. A thin layer of flow with a sharp change in temperature is formed near the wall when the fluid flows through the boundary with a different temperature. Therefore, when the temperature boundary layer is

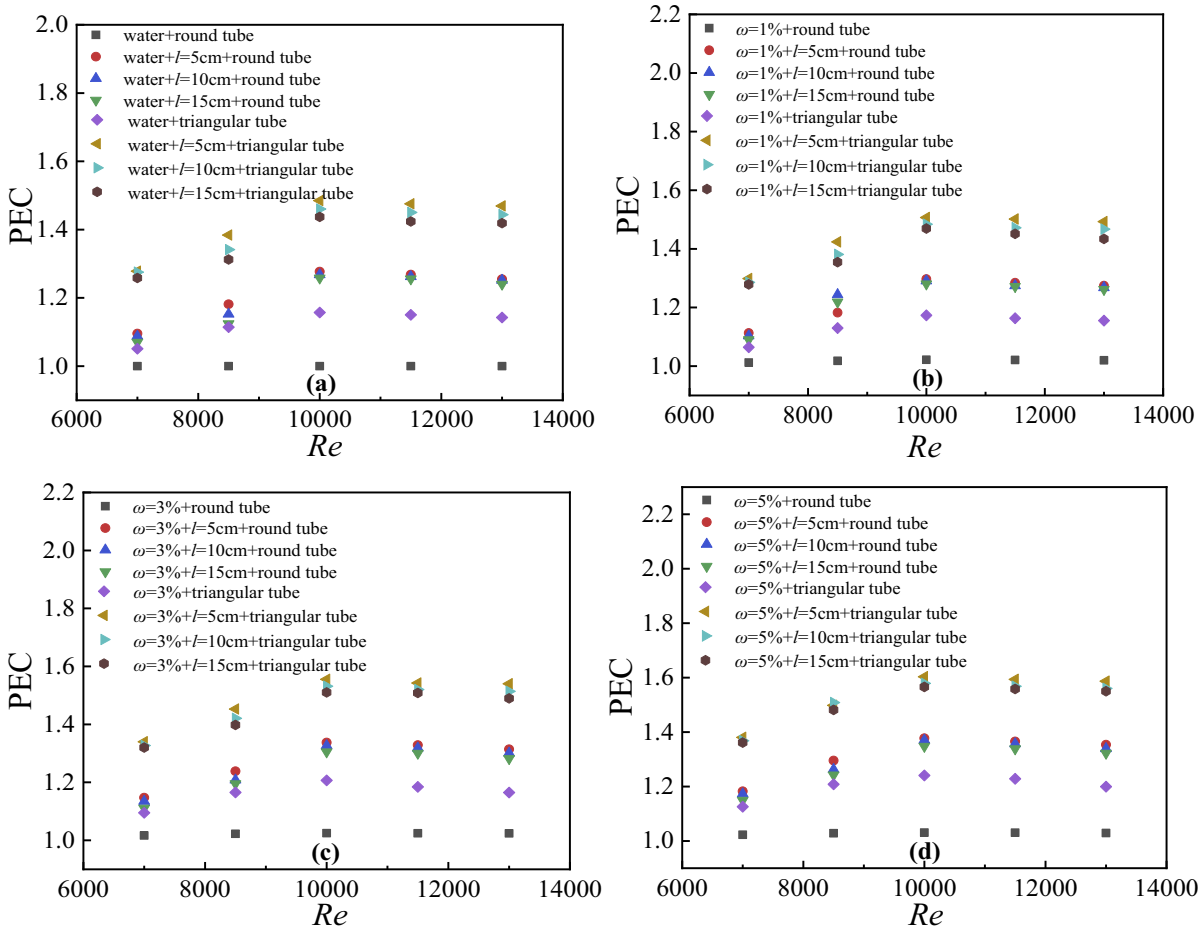

Fig. 25. The effect of hole spacing on PEC comprehensive evaluation index under different mass fractions of SiO_2-H_2O nanofluids: (a) $\varphi = 0\%$, (b) $\varphi = 1\%$, (c) $\varphi = 3\%$, and (d) $\varphi = 5\%$.

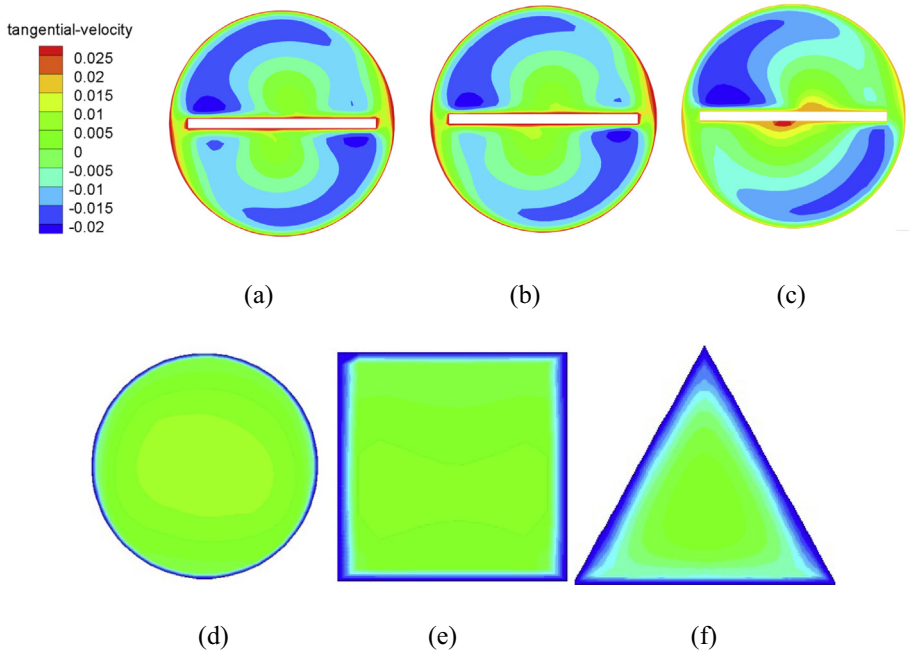

Fig. 26. The influence of different hole shapes on velocity contour of round tubes: (a) round hole, (b) square hole, (c) triangular hole, (d) section of round hole on tape, (e) section of square hole on tape, and (f) section of triangular hole on tape.

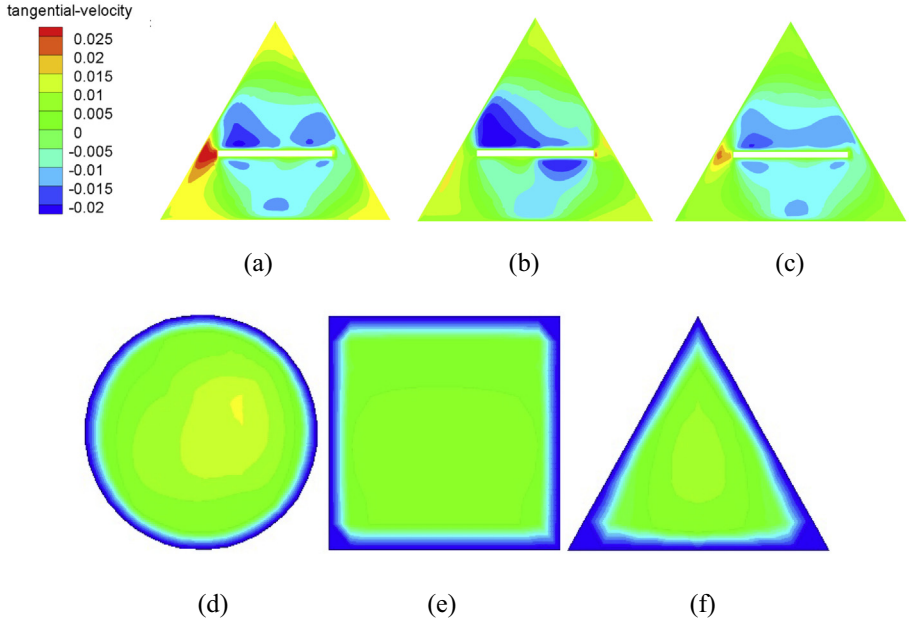

Fig. 27. The influence of different hole shapes on velocity contour of triangular tubes: (a) round hole, (b) square hole, (c) triangular hole, (d) section of round hole on tape, (e) section of square hole on tape, and (f) section of triangular hole on tape.

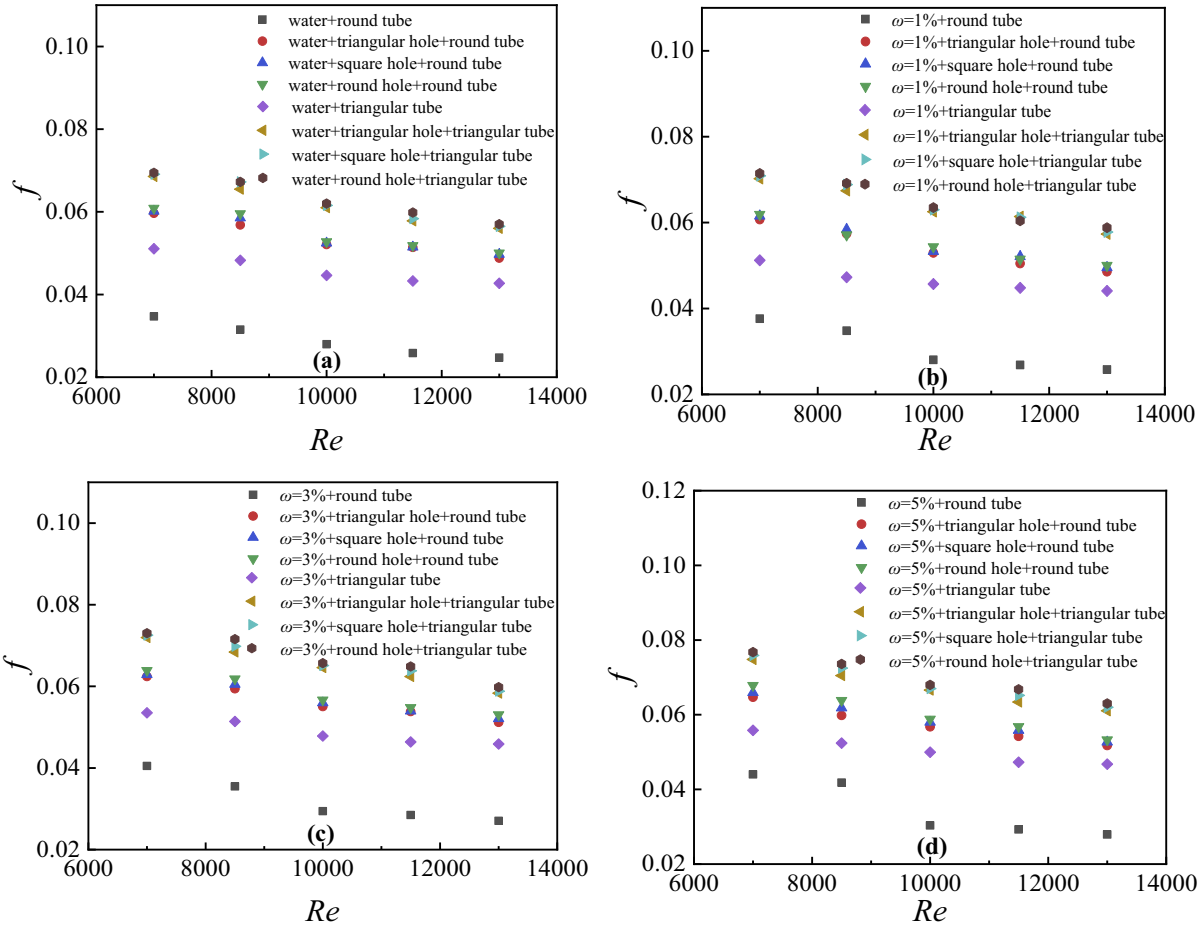

Fig. 28. The effect of hole shape on resistance coefficient under different mass fractions of SiO_2-H_2O nanofluids: (a) $\varphi = 0\%$, (b) $\varphi = 1\%$, (c) $\varphi = 3\%$, and (d) $\varphi = 5\%$.

Table 3
The change of average temperature of fluid with the hole shape.

Hole shape	Round	Square	Triangular
Temperature of flow in round tube (K)	278.1261	278.1183	278.1106
Temperature of flow in triangular tube (K)	282.7017	282.6523	282.6065

thinner, the relatively reduced thermal resistance enhances the heat transfer. However, the triangular tube with a built-in porous twisted tape possesses a thinner temperature boundary layer under turbulence, thus the temperature in the main flow area is higher. The heat exchange efficiency is higher than that of the triangular tube.

Furthermore, the average temperature of fluid also changes. Under the above-mentioned working conditions, the triangular tube exhibits an obvious heat transfer enhancement effect. On the one hand, owing to the turbulent flow of porous twisted tape, the secondary flow is produced, which leads to the thinning of the temperature boundary and strengthening of the flow mixing and heat exchange. On the other hand, the porous twisted tape enlarges the heat exchange surface, thus achieving the purpose of enhancing heat exchange.

At the same time, the Nusselt number shown in Fig. 19 was analyzed, and it was found that the two types of tubes exhibited the same variation trend, which increased with the increase in the Reynolds number. When Reynolds number was 13,000, the Nusselt number of the triangular tube with 5% mass fraction of nanoparticles was 54.83% higher than that of the smooth tube. It indicated that the addition of porous twisted tape and the usage of nanofluids lead to the significant increase in the heat exchange performance of tubes, which can be improved by 55.97% at most in the simulated working conditions. The porous twisted tape makes the flow move radially and tangentially, due to the mixing of the two flows in different directions. The axial flow is under the pressure of radial flow, which leads to the deviation in the original flow track, resulting in the superimposition of the secondary flow on the main flow. This interferes with the original flow and plays a key role in enhancing heat transfer performance to a certain extent. This phenomenon strengthens the mutual mixing of flow and results in thinning of the temperature boundary layer.

The simulation results obtained under different working conditions reveal that the usage of nanofluids, porous twisted tape, and triangular tube can improve the performance of heat exchange in the system to a certain extent. Fig. 20 displays in-depth analysis of PEC comprehensive evaluation index. Comparative analysis indicates that the PEC of the triangular tube with porous twisted tape is the highest, which can reach 1.579 when Reynolds number is 10000 at nanofluids mass fraction of 5%. This configuration scheme of the tube can maximize the objective of heat transfer enhancement.

4. The effects of twisted tape structures

4.1. The effects of hole spacing

In this study, the influence of different hole spacing on flow characteristics was also systematically studied. Notably, the increase of twisted tape hole spacing can improve the heat exchange performance of the system, but it may also bring about the increase of flow resistance. Figs. 21 and 22 display the velocity contours of

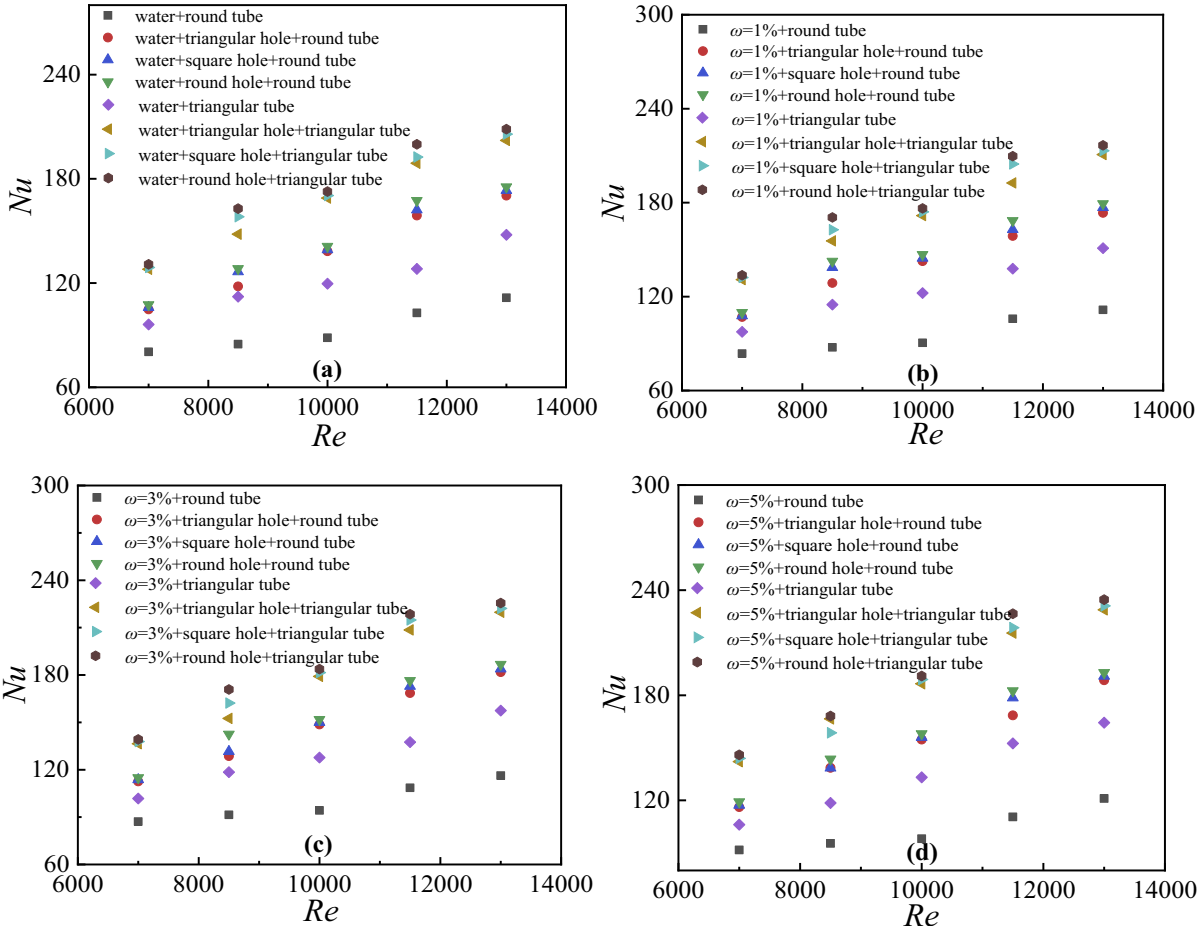

Fig. 29. The effect of hole shape on Nusselt number under different mass fractions of SiO_2-H_2O nanofluids: (a) $\varphi = 0\%$, (b) $\varphi = 1\%$, (c) $\varphi = 3\%$, (d) $\varphi = 5\%$.

round and triangular tubes with different hole spacing, revealing that the flow velocity changes with the hole spacing. Fig. 23 shows the variation curve of flow resistance coefficient in tubes with twisted tapes and different hole spacing (l = 5, 10, and 15 cm). Clearly, the flow resistance of the system increases the most when the hole spacing is 5 cm, and the increase is the least when the hole spacing is 15 cm. Compared to pure water without a built-in porous twisted tape, the resistance coefficient can be increased by 114.89% at most for the twisted tape with a hole spacing of 5 cm. Previous analysis indicates that due to the insertion of the porous twisted tape, the flow produces rotational flow and secondary flow, which can not only enhance the heat exchange effect, but also enlarge the flow resistance to a certain extent. This leads to the increase in the friction of fluid between the tube wall and the porous twisted tape, intensify the collision of fluid molecules, and cause more kinetic energy loss, thus resulting in the increase in the flow resistance.

Furthermore, the heat transfer characteristics of two types of tubes under different twisted tape hole spacing conditions were analyzed. Table 2 summarizes that the average temperature of flow is the highest when twisted tape with the hole spacing of 5 cm is used in either round tube or triangular tube. This phenomenon is mainly attributed to the fact that the holes in twisted tape can increase the disturbance of flow in the tubes, and the decrease of hole spacing makes this disturbance more violent, thus achieving the purpose of enhanced heat exchange.

Fig. 24 also shows the influence of different hole spacing on Nusselt number, which is consistent with the result of the previous research. The results indicate that the heat exchange impact of the system is the best for the hole spacing of 5 cm, and the holes with smaller spacing can interfere the flow to a greater extent, weaken the boundary layer thickness, and reduce the thermal resistance.

Analysis of the variation of PEC comprehensive evaluation index shown in Fig. 25 concludes that the maximum value of PEC is observed when Reynolds number is 10000. Moreover, these results also show that the PEC value increases with the decrease of hole spacing, and the twisted tape with smaller hole spacing can enhance the heat transfer of the system. Noteworthy, the PEC can reach the maximum value of 1.603 when the mass fraction of nanofluids is 5% for the triangular tube with a hole spacing of 5 cm.

4.2. The effects of hole shape

In this study, the flow and heat exchange characteristics of round pipe and triangular pipe with different hole shapes (round hole, square hole, and triangular hole) were also compared and analyzed. Analysis of the velocity contours shown of Figs. 26 and 27 indicates that the change of hole shapes differently impacts the flow velocity of the tubes with the two different shapes. Fig. 28 demonstrates that the flow resistance of the system increases the most when the round hole is drilled on the twisted belt. This may be attributed to the fact that the boundary of the round hole structure has more fluid disturbance, which makes the flow resistance greater.

The heat transfer characteristics of pipelines with different hole shapes were studied when Reynolds number was 7000 and water was used as heat transfer medium. Table 3 summarizes that the average

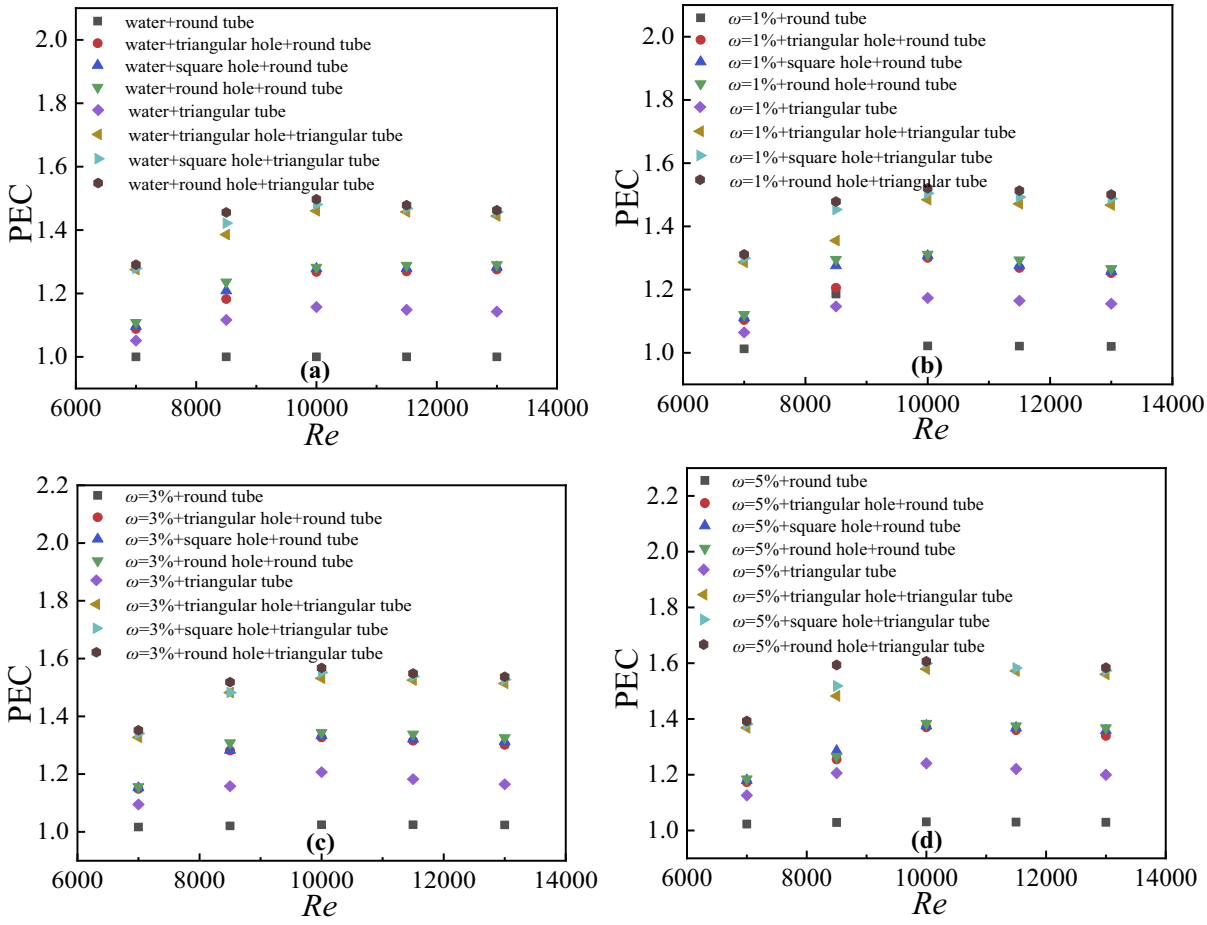

Fig. 30. The effect of hole shape on PEC comprehensive evaluation index under different mass fractions of SiO_2-H_2O nanofluids: (a) $\varphi = 0\%$, (b) $\varphi = 1\%$, (c) $\varphi = 3\%$, and (d) $\varphi = 5\%$.

temperature of fluid is the highest when the twisted tape is punched with round hole. Comparison with Fig. 29 indicates that the Nusselt number also reaches the maximum value when the nanofluids with high mass fraction are used as working medium and round hole is set on the twisted tape, which can be increased by 74.80%. This phenomenon is attributed to the fact that the area of circle is larger than that of square and triangle with the same circumference; as a result, more mixed flows are formed. The round hole generates more eddy currents in the axial flow direction, which improves the average heat transfer [41,42]. This disturbs the flow and increases the Nusselt number to a certain extent. Moreover, it destroys the boundary layer and reduces the heat transfer resistance between the wall and the flow, so as to enhance the heat transfer. At the same time, compared to the acute angle boundary of triangle and square holes, the round holes bring less flow resistance, and better aid in optimization of the PEC comprehensive evaluation index of heat exchange system. According to the PEC comprehensive evaluation index shown in Fig. 30, the PEC reaches the peak when Reynolds number is about 10,000. For triangular tubes with round hole twisted tape, the maximum PEC comprehensive evaluation index is 1.579.

5. Conclusions

In this study, based on the physical model of previous experiments, the numerical models of round tube and triangular tube with different types of twisted tape were established by numerical simulation method. The flow and heat exchange characteristics of twisted tape tubes with different shapes and distances were analyzed. Moreover, the PEC comprehensive evaluation index was studied. The following conclusions are obtained:

(1) The Nusselt number and flow resistance coefficient increase with the increase in the mass fraction of nanofluids. The Nusselt number and flow resistance coefficient also increase by setting the porous twisted tape.
(2) The holes on the twisted tape can strengthen the heat exchange performance, and the flow temperature in the tube decreases with the increase of the hole spacing. At the same time, the enhancement in the Bejan number and entropy in the tube with built-in porous tape is higher than that in the smooth tube.
(3) Whether it is a triangle tube or a round tube, the heat exchange enhancement effect is the best when the twisted tape has round hole than a square hole, and the worst effect is observed for the triangle hole.
(4) For the PEC comprehensive evaluation index, the built-in porous twisted tape and triangular tube can achieve the maximum improvement. The usage of porous twisted tape, nanofluids, and triangular tube can significantly improve the system economy and enhance the heat exchangeability.

Declaration of Competing Interest

The authors declare that they have no known competing financial interests or personal relationships that could have appeared to influence the work reported in this paper.

Acknowledgement

This work was supported by the National Natural Science Foundation of China (Grant no. 51606214); the Natural Science Foundation of Jiangsu Province, China (Grant no. BK20181359).

References

[1] X. Wang, Y. He, M. Chen, Y. Hu, ZnO-Au composite hierarchical particles dispersed oil-based nanofluids for direct absorption solar collectors, Sol. Energy Mater. Sol. Cells 179 (2018) 185–193.
[2] L. Shi, Y. Hu, Y. Bai, Y. He, Dynamic tuning of magnetic phase change composites for solar-thermal conversion and energy storage, Appl. Energy 263 (2020) 114570.
[3] Y. Bie, M. Li, F. Chen, G. Królczyk, Z. Li, Heat transfer mathematical model for a novel parabolic trough solar collecting system with V-shaped cavity absorber, Sustain. Cities Soc. 52 (2020) 101837.
[4] S.M. Parsa, A. Rahbar, M.H. Koleini, S. Aberoumand, M. Afrand, M. Amidpour, A renewable energy-driven thermoelectric-utilized solar still with external condenser loaded by silver/nanofluid for simultaneously water disinfection and desalination, Desalination. 480 (2020) 114354.
[5] K. Bao, C. Hua, X. Wang, X. Han, G. Chen, Experimental investigation on the heat transfer performance and evaporation temperature fluctuation of a new-type metal foam multichannel heat pipe, Int. J. Heat Mass Transf. 154 (2020) 119672.
[6] K. Enoki, M. Ono, T. Okawa, B. Kristiawan, A.T. Wijayanta, Water flow boiling heat transfer in vertical minichannel, Exp. Thermal Fluid Sci. 117 (2020) 110147.
[7] M. Chen, Y. He, Q. Ye, Z. Zhang, Y. Hu, Solar thermal conversion and thermal energy storage of CuO/paraffin phase change composites, Int. J. Heat Mass Transf. 130 (2019) 1133–1140.
[8] M. Huang, H. Borzoei, A. Abdollahi, Z. Li, A. Karimipour, Effect of concentration and sedimentation on boiling heat transfer coefficient of GNPs-SiO_2/deionized water hybrid Nanofluid: an experimental investigation, Int. Commun. Heat Mass Transf. 122 (2021) 105141.
[9] X. Ma, M. Sheikholeslami, M. Jafaryar, A. Shafee, T. Nguyen-Thoi, Z. Li, Solidification inside a clean energy storage unit utilizing phase change material with copper oxide nanoparticles, J. Clean. Prod. 245 (2020) 118888.
[10] X. Zhai, C. Qi, Y. Yang, J. Wang, Thermo-hydraulic performance of nanofluids under adjustable magnetic field, Appl. Therm. Eng. 186 (2021) 116491.
[11] C. Qi, C. Li, G. Zhao, M. Liu, D. Han, Influence of rotation angle of a triangular tube with a built-in twisted tape on the thermal-exergy efficiency and entropy generation of nanofluids in the heat exchange system, Asia-Pacific J. Chem. Eng. 15 (2020), e2401.
[12] M. Sheikholeslami, H. Keramati, A. Shafee, Z. Li, O.A. Alawad, I. Tlili, Nanofluid MHD forced convection heat transfer around the elliptic obstacle inside a permeable lid drive 3D enclosure considering lattice Boltzmann method, Phys. A. 523 (2019) 87–104.
[13] Y. Zhai, L. Li, J. Wang, Z. Li, Evaluation of surfactant on stability and thermal performance of Al_2O_3-ethylene glycol (EG) nanofluids, Powder Technol. 343 (2019) 215–224.
[14] M. Ma, Y. Zhai, P. Yao, Y. Li, H. Wang, Synergistic mechanism of thermal conductivity enhancement and economic analysis of hybrid nanofluids, Powder Technol. 373 (2020) 702–715.
[15] X. Liu, D. Toghraie, M. Hekmatifar, O.A. Akbari, A. Karimipour, M. Afrand, Numerical investigation of nanofluid laminar forced convection heat transfer between two horizontal concentric cylinders in the presence of porous medium, J. Therm. Anal. Calorim. 141 (2020) 2095–2108.
[16] S. Nazari, M. Bahiraei, H. Moayedi, H. Safarzadeh, A proper model to predict energy efficiency, exergy efficiency, and water productivity of a solar still via optimized neural network, J. Clean. Prod. 277 (2020) 123232.
[17] M. Bahiraei, S. Nazari, H. Safarzadeh, Modeling of energy efficiency for a solar still fitted with thermoelectric modules by ANFIS and PSO-enhanced neural network: a nanofluid application, Powder Technol. 385 (2021) 185–198.
[18] A.T. Wijayanta Pranowo, Numerical solution strategy for natural convection problems in a triangular cavity using a direct meshless local Petrov-Galerkin method combined with an implicit artificial-compressibility model, Eng. Anal. Bound. Elem. 126 (2021) 13–29.
[19] N.N. Esfahani, D. Toghraie, M. Afrand, A new correlation for predicting the thermal conductivity of ZnO–Ag (50%–50%)/water hybrid nanofluid: an experimental study, Powder Technol. 323 (2018) 367–373.
[20] Y. Hu, B. Zhang, K. Tan, Y. He, J. Zhu, Regulation of natural convection heat transfer for SiO_2–solar salt nanofluids by optimizing rectangular vessels design, Asia-Pacific J. Chem. Eng. 15 (2020), e2409.
[21] H. Sajjadi, A.A. Delouei, R. Mohebbi, M. Izadi, S. Succi, Natural convection heat transfer in a porous cavity with sinusoidal temperature distribution using Cu/water nanofluid: double MRT lattice boltzmann method, Commun. Comput. Phys. 29 (2020) 292–318.
[22] L. Shi, Y. Hu, Y. He, Magneto-responsive thermal switch for remote-controlled locomotion and heat transfer based on magnetic nanofluid, Nano Energy 71 (2020) 104582.
[23] M. Bahiraei, S. Heshmatian, Electronics cooling with nanofluids: a critical review, Energy Convers. Manag. 172 (2018) 438–456.
[24] J. Alsarraf, A. Shahsavar, M. Khaki, R. Ranjbarzadeh, A. Karimipour, M. Afrand, Numerical investigation on the effect of four constant temperature pipes on natural cooling of electronic heat sink by nanofluids: a multifunctional optimization, Adv. Powder Technol. 31 (2020) 416–432.
[25] C. Qi, Y. Wang, J. Tang, Effect of squid fin bionic surface and magnetic nanofluids on CPU cooling performance under magnetic field, Asia-Pacific J. Chem. Eng. 15 (2020), e2482.
[26] S.R. Yan, A. Hajatzadeh Pordanjani, S. Aghakhani, A. Shahsavar Goldanlou, M. Afrand, Managment of natural convection of nanofluids inside a square enclosure by different nano powder shapes in presence of fins with different shapes and magnetic field effect, Adv. Powder Technol. 31 (2020) 2759–2777.
[27] M. Sheikholeslami, A. Zeeshan, A. Majeed, Control volume based finite element simulation of magnetic nanofluid flow and heat transport in non-Darcy medium, J. Mol. Liq. 268 (2018) 354–364.
[28] A. Hajatzadeh Pordanjani, S. Aghakhani, A. Karimipour, M. Afrand, M. Goodarzi, Investigation of free convection heat transfer and entropy generation of nanofluid

flow inside a cavity affected by magnetic field and thermal radiation, J. Therm. Anal. Calorim. 137 (2019) 997–1019.
[29] B. Kristiawan, B. Santoso, A.T. Wijayanta, M. Aziz, T. Miyazaki, Heat transfer enhancement of TiO_2/water nanofluid at laminar and turbulent flows: a numerical approach for evaluating the effect of nanoparticle loadings, Energies. 11 (2018) 1584.
[30] B. Kristiawan, A.I. Rifa'i, K. Enoki, A.T. Wijayanta, T. Miyazaki, Enhancing the thermal performance of TiO_2/water nanofluids flowing in a helical microfin tube, Powder Technol. 376 (2020) 254–262.
[31] M. Hemmat Esfe, H. Rahimi Raki, M.R. Sarmasti Emami, M. Afrand, Viscosity and rheological properties of antifreeze based nanofluid containing hybrid nanopowders of MWCNTs and TiO_2 under different temperature conditions, Powder Technol. 342 (2019) 808–816.
[32] I. Kazemi, M. Sefid, M. Afrand, A novel comparative experimental study on rheological behavior of mono & hybrid nanofluids concerned graphene and silica nanopowders: characterization, stability and viscosity measurements, Powder Technol. 366 (2020) 216–229.
[33] S. Sarboolookzadeh Harandi, A. Karimipour, M. Afrand, M. Akbari, A. D'Orazio, An experimental study on thermal conductivity of F-MWCNTs-Fe_3O_4/EG hybrid nanofluid: effects of temperature and concentration, Int. Commun. Heat Mass Transf. 76 (2016) 171–177.
[34] M. Hemmat Esfe, S. Wongwises, A. Naderi, A. Asadi, M.R. Safaei, H. Rostamian, M. Dahari, A. Karimipour, Thermal conductivity of Cu/TiO_2-water/EG hybrid nanofluid: experimental data and modeling using artificial neural network and correlation, Int. Commun. Heat Mass Transf. 66 (2015) 100–104.
[35] Z. Li, S. Asadi, A. Karimipour, A. Abdollahi, I. Tlili, Experimental study of temperature and mass fraction effects on thermal conductivity and dynamic viscosity of SiO_2-oleic acid/liquid paraffin nanofluid, Int. Commun. Heat Mass Transf. 110 (2020) 104436.
[36] A. Shafee, A. Arabkoohsar, M. Sheikholeslami, M. Jafaryar, M. Ayani, T. Nguyen-Thoi, D.B. Basha, I. Tlili, Z. Li, Numerical simulation for turbulent flow in a tube with combined swirl flow device considering nanofluid exergy loss, Phys. A. 542 (2020) 122161.
[37] W. He, R. Mashayekhi, D. Toghraie, O.A. Akbari, Z. Li, I. Tlili, Hydrothermal performance of nanofluid flow in a sinusoidal double layer microchannel in order to geometric optimization, Int. Commun. Heat Mass Transf. 117 (2020) 104700.
[38] M. Izadi, R. Mohebbi, A.A. Delouei, H. Sajjadi, Natural convection of a magnetizable hybrid nanofluid inside a porous enclosure subjected to two variable magnetic fields, Int. J. Mech. Sci. 151 (2019) 154–169.
[39] S.A.M. Mehryan, M.A. Sheremet, M. Soltani, M. Izadi, Natural convection of magnetic hybrid nanofluid inside a double-porous medium using two-equation energy model, J. Mol. Liq. 277 (2019) 959–970.
[40] M. Izadi, S. Sinaei, S.A.M. Mehryan, H.F. Oztop, N. Abu-Hamdeh, Natural convection of a nanofluid between two eccentric cylinders saturated by porous material: Buongiorno's two phase model, Int. J. Heat Mass Transf. 127 (2018) 67–75.
[41] A.T. Wijayanta, M. Aziz Mirmanto, Heat transfer augmentation of internal flow using twisted tape insert in turbulent flow, Heat Transf. Eng. 41 (2020) 1288–1300.
[42] A.T. Wijayanta, Mirmanto Pranowo, B. Kristiawan, M. Aziz, Internal flow in an enhanced tube having square-cut twisted tape insert, Energies 12 (2019) 306.
[43] I. Yaningsih, A.T. Wijayanta, T. Miyazaki, S. Koyama, V-cut twisted tape insert effect on heat transfer enhancement of single phase turbulent flow heat exchanger, AIP Conf. Proc. 1931 (2018), 030038.
[44] C. Qi, F. Fan, Y. Pan, M. Liu, Y. Yan, Effects of turbulator with round hole on the thermo-hydraulic performance of nanofluids in a triangle tube, Int. J. Heat Mass Transf. 146 (2020) 118897.
[45] C. Qi, T. Luo, M. Liu, F. Fan, Y. Yan, Experimental study on the flow and heat transfer characteristics of nanofluids in double-tube heat exchangers based on thermal efficiency assessment, Energy Convers. Manag. 197 (2019) 111877.
[46] X. Wang, X. Yan, N. Gao, G. Chen, Prediction of thermal conductivity of various nanofluids with ethylene glycol using artificial neural network, J. Therm. Sci. 29 (2020) 1504–1512.
[47] X. Wang, B. Li, Y. Yan, N. Gao, G. Chen, Predicting of thermal resistances of closed vertical meandering pulsating heat pipe using artificial neural network model, Appl. Therm. Eng. 149 (2019) 1134–1141.
[48] X. Wang, Y. Yan, X. Meng, G. Chen, A general method to predict the performance of closed pulsating heat pipe by artificial neural network, Appl. Therm. Eng. 157 (2019) 113761.
[49] M. Bahiraei, N. Mazaheri, M.R. Daneshyar, Employing elliptical pin-fins and nanofluid within a heat sink for cooling of electronic chips regarding energy efficiency perspective, Appl. Therm. Eng. 183 (2021) 116159.
[50] M. Bahiraei, M. Naseri, A. Monavari, A CFD study on thermohydraulic characteristics of a nanofluid in a shell-and-tube heat exchanger fitted with new unilateral ladder type helical baffles, Int. Commun. Heat Mass Transf. 124 (2021) 105248.
[51] V. Gnielinski, New equations for heat mass transfer in turbulent pipe and channel flows, Int. Chem. Eng. 16 (1976) 359–368.
[52] B. Sun, A. Yang, D. Yang, Experimental study on the heat transfer and flow characteristics of nanofluids in the built-in twisted belt external thread tubes, Int. J. Heat Mass Transf. 107 (2017) 712–722.
[53] S. Kimura, A. Bejan, The "heatline" visualization of convective heat transfer, J. Heat Transf. 105 (1983) 916–919.
[54] A. Bejan, Entropy Generation through Heat and Fluid Flow, Wiley, New York, 1982.